# Influence of tin doping and annealing on structural and optical properties of nickel oxide thin films prepared via spray pyrolysis

G. D. Salman a, K. I. Hassoon b,\*, M. A. Hassan c

Sciences, University of Technology, Baghdad, Iraq

Nickel oxide (NiO) is a p-type semiconductor with applications in optoelectronics, such as solar cells and photo detectors. This study explores the effects of Sn doping and annealing on NiO thin films, prepared using a cost-effective spray pyrolysis method. Doping concentrations of 3%, 6%, and 9% Sn were tested, and annealing at 500°C improved structural properties. XRD confirmed crystallinity, and the bandgap increased with doping, enhancing electronic properties. Urbach energy values indicated improved optoelectronic potential, contributing insights for optimizing NiO-based devices, particularly in solar cell applications. The findings emphasize NiO's viability for advanced optoelectronic technologies.

(Received June 9, 2025; Accepted September 26, 2025)

*Keywords:* Thin films, Nickel oxide, Single crystal, Spray pyrolysis, Direct band gap, Urbach energy, Sublimation

#### 1. Introduction

Nickel oxide compounds possess a wide range of unique properties, making them suitable for diverse applications. These include gas sensors [1], solar cells [2,3], electron blocking layers [4, 5], current spreading layers [6]. Additionally, NiO plays a role in p-n junctions [7, 8], catalysts [9], fuel cells [10], and battery electrodes [11]. Its electrochromic behavior allows for change color under applied electric charge, and its high theoretical capacity makes it valuable for supercapacitors and lithium-ion batteries [12,13].

Many doped metal oxide semiconductors, such as indium tin oxide (ITO), fluorine-doped tin oxide (FTO), and Al-doped zinc oxides, are crucial transparent conductive oxides (TCO) used in perovskite solar cells, dye-sensitized solar cells, optical detectors, and other optoelectronic devices. Notably, all these materials are n-type semiconductors [14-16]. However, some applications require a p-type semiconductor with high transmittance in the visible region. Nickel oxide is one of the few that fits this description. Compared to n-type materials, fewer studies have focused on p-type transparent metal oxide films [17]. Most p-type materials lack the required combination of high electrical conductivity and transparency for commercial or industrial use. Therefore, developing high-performance p-type semiconductors is essential [18, 19]. NiO offers additional advantages like a wide band gap (3.5 - 4 eV), cost-effectiveness, and excellent durability [20, 21]. Doping typically causes deviations from stoichiometry and increases defects but enhances some optical properties. In this study, we used low-cost spray pyrolysis to prepare highly crystalline undoped and Sn-doped NiO thin films and examined the effect of doping on transmittance, absorption coefficient, energy bandgap and Urbach energy.

CSP was selected for its lower cost compared to vacuum-based deposition techniques like RF magnetron sputtering and thermal evaporation (TE), which require expensive vacuum facilities. Furthermore, previous studies [22,24] have demonstrated that the CSP technique can be optimized

<sup>&</sup>lt;sup>a</sup> Institute of Technology, Middle Technical University, Baghdad, Iraq

<sup>&</sup>lt;sup>b</sup> Department of Laser Science and Technology, College of Applied

<sup>&</sup>lt;sup>c</sup> Department of Medical and Industrial Materials Science, College of Applied Sciences, University of Technology, Baghdad, Iraq

<sup>\*</sup> Corresponding author: khaleel.i.hassoon@uotechnology.edu.iq https://doi.org/10.15251/DJNB.2025.203.1153

to produce smooth and homogeneous thin films through specific experimental strategies, which will be discussed in detail in the following section.

# 2. Experimental part

Distilled water and ethanol were used to clean the quartz substrates. Pure nickel chloride salt (NiCl<sub>2</sub> 6H<sub>2</sub>O, 99.5% purity) was dissolved in distilled water to prepare a 0.1 M concentration. The doping process was implemented by adding a solution of tin chloride (purity 98% from Sigma-Aldrich) with the same concentration of nickel chloride at different ratios (3%, 6%, 9%).

The nickel oxide thin films were deposited on the quartz substrate using the tilt spray pyrolysis setup. The temperature of the heater surface was set to 400°C. As mentioned above, the spray angle was a 45°. This angle required a 30 cm distance between the nozzle and the substrate. Unlike a vertical spray setup (zero-angle), the 45° tilt angle allows finer droplets to form and deposit more evenly on the substrate, improving film quality (Figure 1). The quantitative enhancement in crystallinity is provided in Table 1.

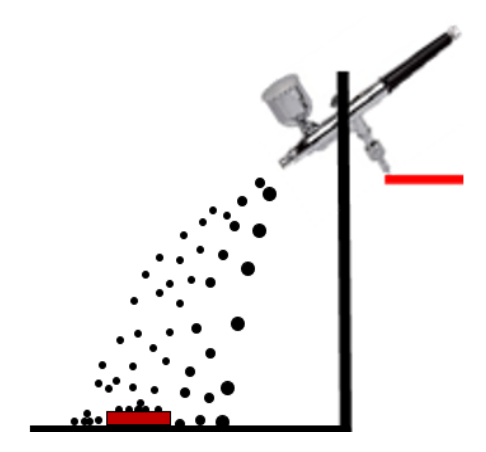


Fig. 1. Using tilt angle deposition, finer droplets are expected to be deposited on the substrate.

The time for one spray was 3 seconds, and the stopping time between each two sprays was 30 seconds. The films must not be removed from the heater until they cool down to room temperature. The chemical interaction leading to the formation of NiO proceeds as follows:

When NiCl<sub>2</sub>·6H<sub>2</sub>O is dissolved in distilled water, it dissociates into nickel(II) ions and chloride ions:

$$NiCl_2 \cdot 6H_2O \rightarrow Ni^{2+} + 2Cl^- + 6H_2O$$

Then, Nickel(II) ions react with water and a base to form nickel hydroxide (Ni(OH)<sub>2</sub>):

$$Ni^{2+} + 2OH^- \rightarrow Ni(OH)_2 \downarrow$$

Upon heating (annealing at 400 °C), nickel hydroxide undergoes thermal decomposition, releasing water vapor and forming nickel oxide (NiO):

$$Ni(OH)_2 \xrightarrow{\Delta} NiO + H_2O \uparrow$$

Our chemical spraying pyrolysis setup (Figure 2) is enhanced to obtain homogeneous and smooth thin films via the following tactics: 1. Using an inclined spraying angle (45°) between the spraying nozzle and the sample surface 2. Utilizing exceptionally fine nozzles taken from an atomizer 3. Setting an electronic regulator to control the spraying time and 4. Manually rotating

every three sprays to obtain better uniformity. This CPS setup enhances film crystallinity and smoothness, producing surfaces comparable or superior to conventional CSP, RFMS, TE, and e-Beam deposition methods, as verified through XRD analysis.

After the deposition process, the films were annealed at a temperature of 500°C for 2 hours without vacuum to enhance the structural properties.

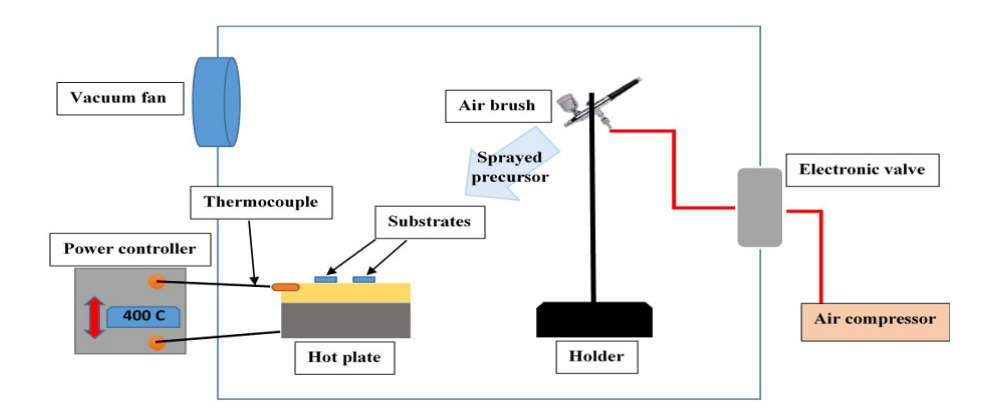


Fig. 2. Spray pyrolysis system schematic diagram.

To confirm the sublimation of Sn atoms from Sn-doped NiO thin films during the annealing process, empty glass slides were placed beside the films inside a Pyrex dish. After annealing, the empty slides were covered with SnO<sub>2</sub> film due to the sublimation of Sn and the interaction of Sn with oxygen as shown in Figure 3.

An EDX test is performed on the glass substrate covered with SnO<sub>2</sub> to verify the sublimation process of tin oxide. Samples were labeled as NS0, NS3, NS6, and NS9 for NiO films doped with 0%, 3%, 6%, and 9% Sn, respectively. For sublimated SnO<sub>2</sub> deposits, labels S3, S6, and S9 were used, corresponding to NiO films doped with 3%, 6%, and 9% Sn.

Using X-ray diffraction (XRD, Shimadzu 6000), the structural characteristics of both undoped and doped NiO films were determined for  $2\theta$  in the range of  $10^{\circ}$ – $90^{\circ}$  and wavelength  $\lambda$ =0.15406 nm (Cu-K $\alpha$ ). The morphology of the films was examined with a field emission scanning electron microscope (TESCAN MIRA3). The thickness is measured from a cross-section image of the field emission scanning electron microscope (FESEM). The optical parameters for both undoped and doped NiO films were calculated from UV-VIS measurements in the wavelength range 200–1200 nm using a Metertech SP8001 spectrophotometer.

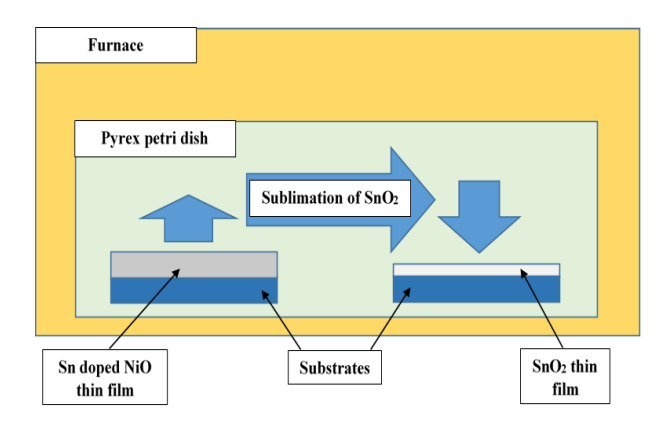


Fig. 3. Schematic diagram of the Sn sublimation method.

#### 3. Results and discussion

# 3.1. Structural properties (XRD)

Structural properties have a significant impact on the behavior of NiO thin film on optoelectronic devices. Figure 4 shows the patterns of XRD for undoped, and tin-doped nickel oxide films prepared by CSP method. The undoped NiO and Sn doped (3%) films (Figure 4a and 4b) show high crystallanity which is rather uncommon for the as-deposited NiO films prepared by CPS [26-28]. In general, the films show a preferred diffraction angle at  $2\theta = 37.2^{\circ}$  corresponding to plane (111).

Compared with previous data, high crystallanity is an unexpected feature for NiO thin films prepared by spray pyrolysis method. However, both the height and the FWHM of (111) peak, which are two important parameters of crystallinity are better than those prepared earlier by CSP [29-31], or even by sputtering [32-36] or e-Beam evaporation [36]. We think that this is due to the effective preparation tactics mentioned in the experimental part.

There are also two small peaks at diffraction angles  $43.2^{\circ}$ ,  $79.4^{\circ}$  corresponding to planes (200) and (222) respectively. According to JCPDS Card no.04-0835 (cf. Table 1), the crystalline structure for our prepared NiO thin films is Face-centered cubic (FCC). These results agree well with earlier works [1,23].

The figure also reveals that the intensity corresponding to plane (111) decreases in height when the amount of Sn dopant increases. This is due to the defects generated because of the doping and the sublimation processes of Sn atoms. Moreover, the small peak corresponding to plane (222) begins to fade when the Sn dopant increases until it fully disappears at a rate of 9% Sn.

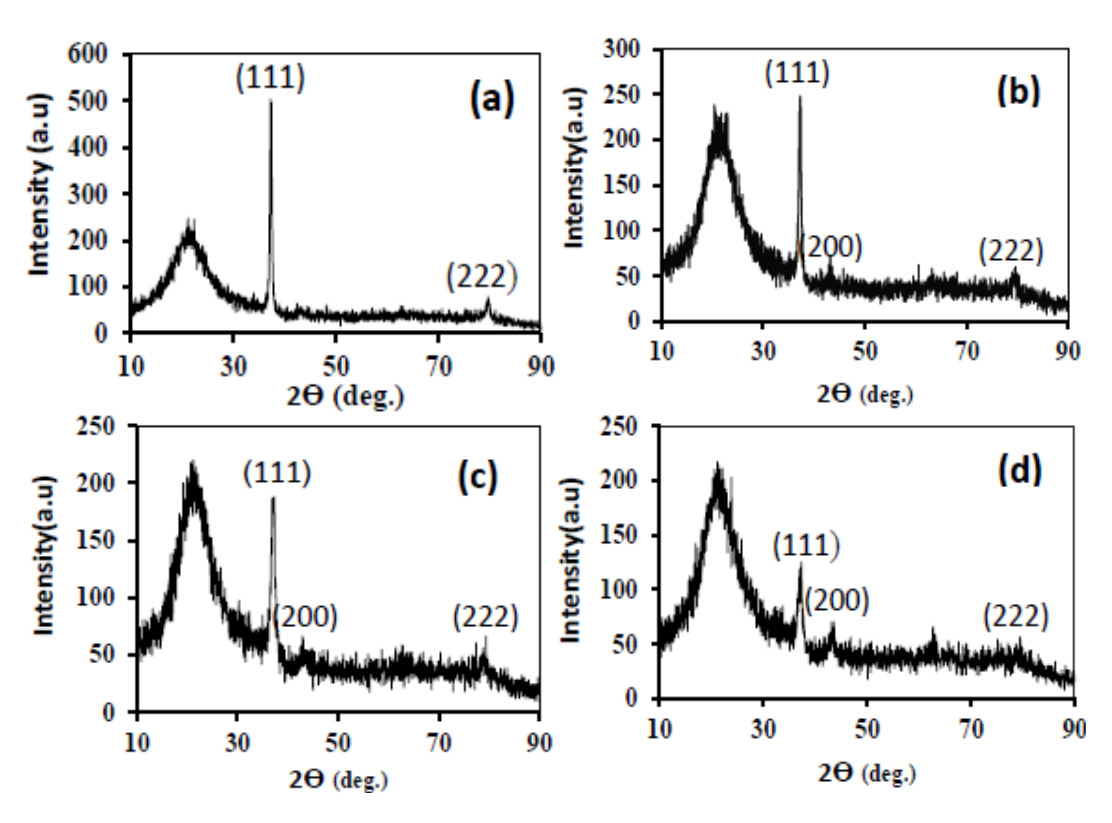


Fig. 4. XRD analysis for (a) undoped NiO (NS0) (b) 3%Sn:NiO (NS3) (c) 6%Sn:NiO (NS6) (d) 9%Sn:NiO (NS9) films.

In Sn-doped NiO thin films prepared by spray pyrolysis, the primary types of defects that can form include: (a) Substitutional Defects - Since Sn atoms replace Ni atoms in the NiO lattice, substitutional doping is the dominant defect type. This can lead to lattice distortion due to the size

difference between Sn and Ni ions [37]. (b) Vacancies - The doping process and subsequent annealing can create nickel vacancies ( $V_{Ni}$ ), which influence electrical conductivity and optical properties. These vacancies can enhance p-type conductivity by increasing hole concentration [38]. (c) Interstitial Defects - While less common, some Sn atoms may occupy interstitial sites, leading to local strain in the crystal structure [39]. (d) Oxygen Deficiencies - Depending on the deposition conditions, oxygen vacancies ( $V_0$ ) may form, affecting optical absorption and electrical behavior.[39].

Considering the first peak at  $2\theta$ =37.3°, the table reveals that the undoped NiO thin films have the highest value of crystal size, thinest FWHM for (111) plane and lowest value of defects density.

The average crystallite size (D) was calculated using Scherer's formula (Eq.(1) [36].

$$D = \frac{K\lambda}{\beta \cos \theta} \tag{1}$$

where K is a constant that typically equals to (0.9),  $\lambda$  is the incident radiation wavelength (0.15406 nm) for  $(CuK\alpha)$ ,  $\beta$  is the full width half maximum of the peak (in radians). The defects density was calculated according to Eq. (2) [40 -42].

$$\delta = \frac{1}{D^2} \tag{2}$$

The results of XRD for undoped and doped NiO thin films are summarized in Table (1). Considering the first peak at  $2\theta=37.3^{\circ}$ , the table reveals that the undoped NiO thin films have the highest value of crystal size, thinest FWHM for (111) plane and lowest value of defects density.

| Samples | Description | 2θ(deg) | hkl | β=FWHM | D(cm)             | $\delta = 1/D^2 \text{ (cm}^{-2})$ | JCPDS      |
|---------|-------------|---------|-----|--------|-------------------|------------------------------------|------------|
| name    |             |         |     | (deg)  | ×10 <sup>-6</sup> | × 10 <sup>11</sup>                 | Card       |
| NS0     | NiO undoped | 37.3    | 111 | 0.436  | 1.93              | 2.70                               | No. 04-    |
|         |             | 79.5    | 222 | 0.673  | 1.54              | 4.23                               | 0835       |
| NS3     | 3%Sn :NiO   | 37.2    | 111 | 0.540  | 1.55              | 4.14                               | 2θ(Miller  |
|         |             | 43.1    | 200 | 0.353  | 2.42              | 1.70                               | indices):  |
|         |             | 79.6    | 222 | 0.320  | 3.24              | 0.96                               | 37.7 (111) |
| NS6     | 6%Sn :NiO   | 37.11   | 111 | 1.226  | 0.68              | 21.35                              | 43.1 (200) |
|         |             | 43.03   | 200 | 1.360  | 0.63              | 25.30                              | 62.9 (220) |
|         |             | 79.02   | 222 | 1.060  | 0.97              | 10.57                              | 75.4 (311) |
| NS9     | 9%Sn :NiO   | 37.17   | 111 | 1.160  | 0.72              | 19.11                              | 79.4(222)  |
|         |             | 43.19   | 200 | 1.360  | 0.63              | 25.27                              | Space      |
|         |             |         |     |        |                   |                                    | Group:     |
|         |             |         |     |        |                   |                                    | Fm-3m      |
|         |             |         |     |        |                   |                                    | Lattice    |
|         |             |         |     |        |                   |                                    | Parameter: |
|         |             |         |     |        |                   |                                    | 0.417 nm   |

Table 1. The crystal parameters of NiO undoped and doped films.

#### 3.2. Morphological study and EDS analysis

Figure 5 displays a cross-section image of field emission scanning electron microscope (FESEM). The image was used to calculate the average thickness of the NiO film on glass substrate. The white arrow indicates that the average thickness of NiO thin film deposited on glass substrate is about 690 nm.

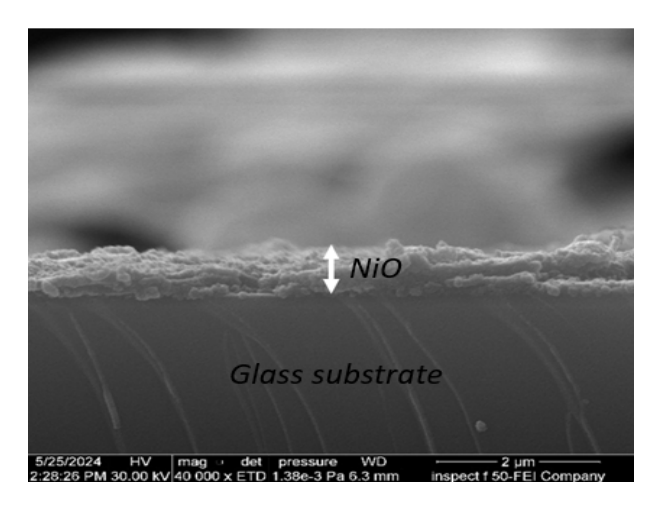


Fig. 5. The cross-sectional SEM image of NiO thin film deposited on glass substrate.

Figure 6 shows FESEM images for undoped and Sn-doped NiO thin films. No remarkable changes can be observed, and it seems that the doping process did not affect the grain shapes in the NiO films. The scanned areas show grains of irregular shapes with varied sizes. This result is consistent with reference [43].

However, as the dopants increase, the irregularity increases too, and at high doping concentrations of samples NS6 and NS9, void and crack-like features appear on the films because of the sublimation Sn atoms. This result is compatible with the X-ray and the coming absorption coefficient results.

Energy-dispersive X-ray spectroscopy test (EDX) is conducted to identify the elemental components of the prepared NiO films before and after doping. Figure 7 shows that the essential elemental components of the prepared NiO thin films are Ni and O elements for the undoped NiO films and Ni, O and Sn elements for tin doped NiO films. The Si component comes from the glass substrate (SiO<sub>2</sub>).

Table 2 shows that the weight ratio for NS9 is (1.6) which is lower than those for NS3 and NS6. This unexpected result may be due to the sublimation of Sn during the annealing process at temperature 500 °C for 2h. Moreover, EDX is employed to confirm the deposition of SnO<sub>2</sub> on glass after sublimation during the annealing process.

As shown earlier in Figure 3, during the annealing process, bare glass substrates were put beside the Sn doped NiO samples. After annealing, all the bare glass substrates were covered by layers of SnO<sub>2</sub>. Figure 8 shows EDX for S3, S6, and S9 samples and confirms that the essential components of these layers are Sn and O. These results suggest the following sinario: During the anealing process at rather high temperature (500 °C), the Sn atoms sublimate from Sn doped films into the air, next Sn atoms combine with O<sub>2</sub> in the air inside the furnace and form SnO<sub>2</sub> gas molecules.

Finally, the SnO<sub>2</sub> gas molecules are deposited onto the glass substrate to form SnO<sub>2</sub> layer. This sinario is supported by the fact that pure Sn element evaporates very rapidly at temperatures higher than its melting point (231.93 °C). The above results are consistent with a previous work [45]. The deposition of SnO<sub>2</sub> layers because of sublimation effect can be considered a promising novel method to prepare low cost SnO<sub>2</sub> thin films.

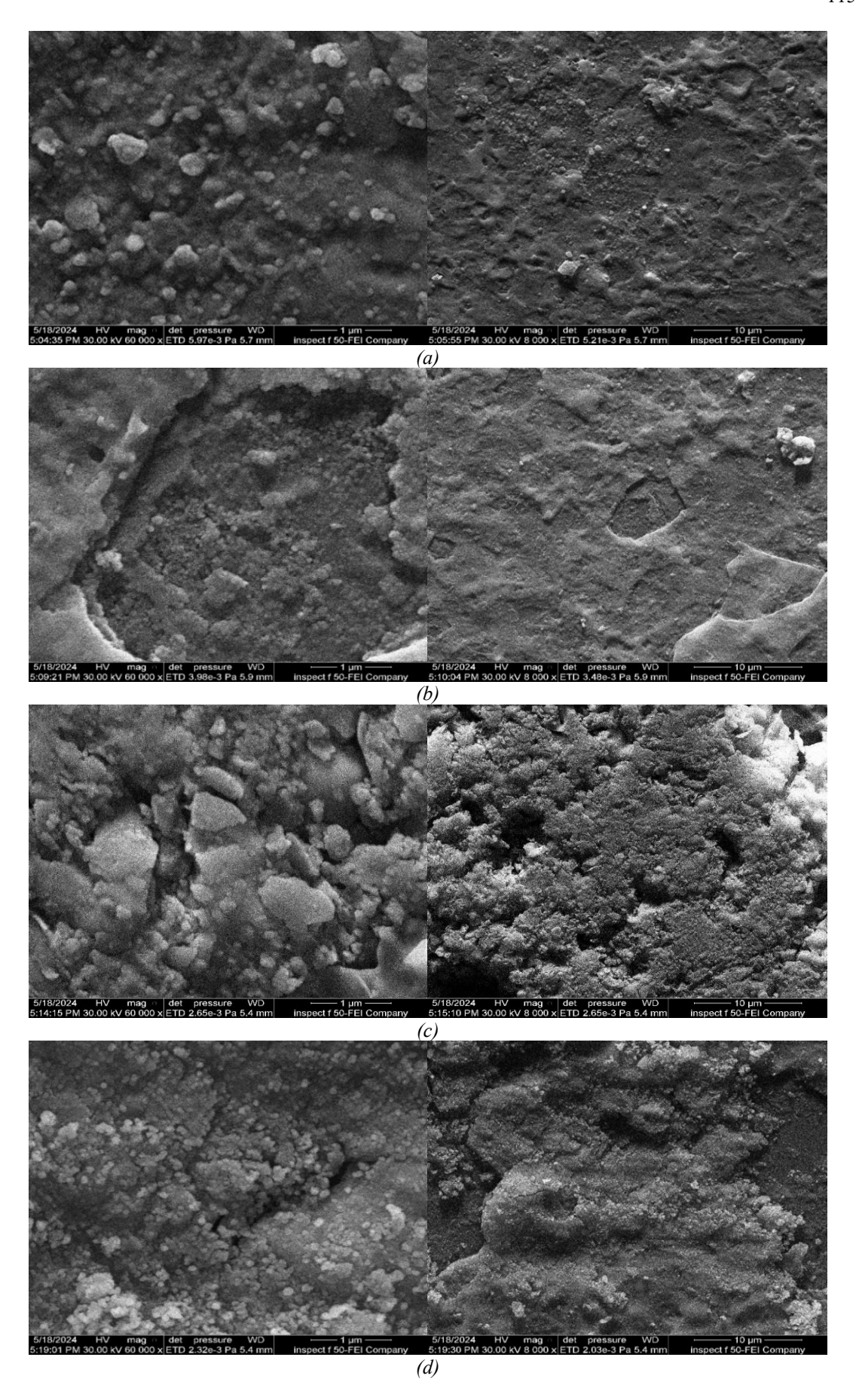


Fig. 6. SEM images of (a) NiO, (b) NiO: 3% Sn, (c) NiO: 6% Sn and (d) NiO:9% Sn films.

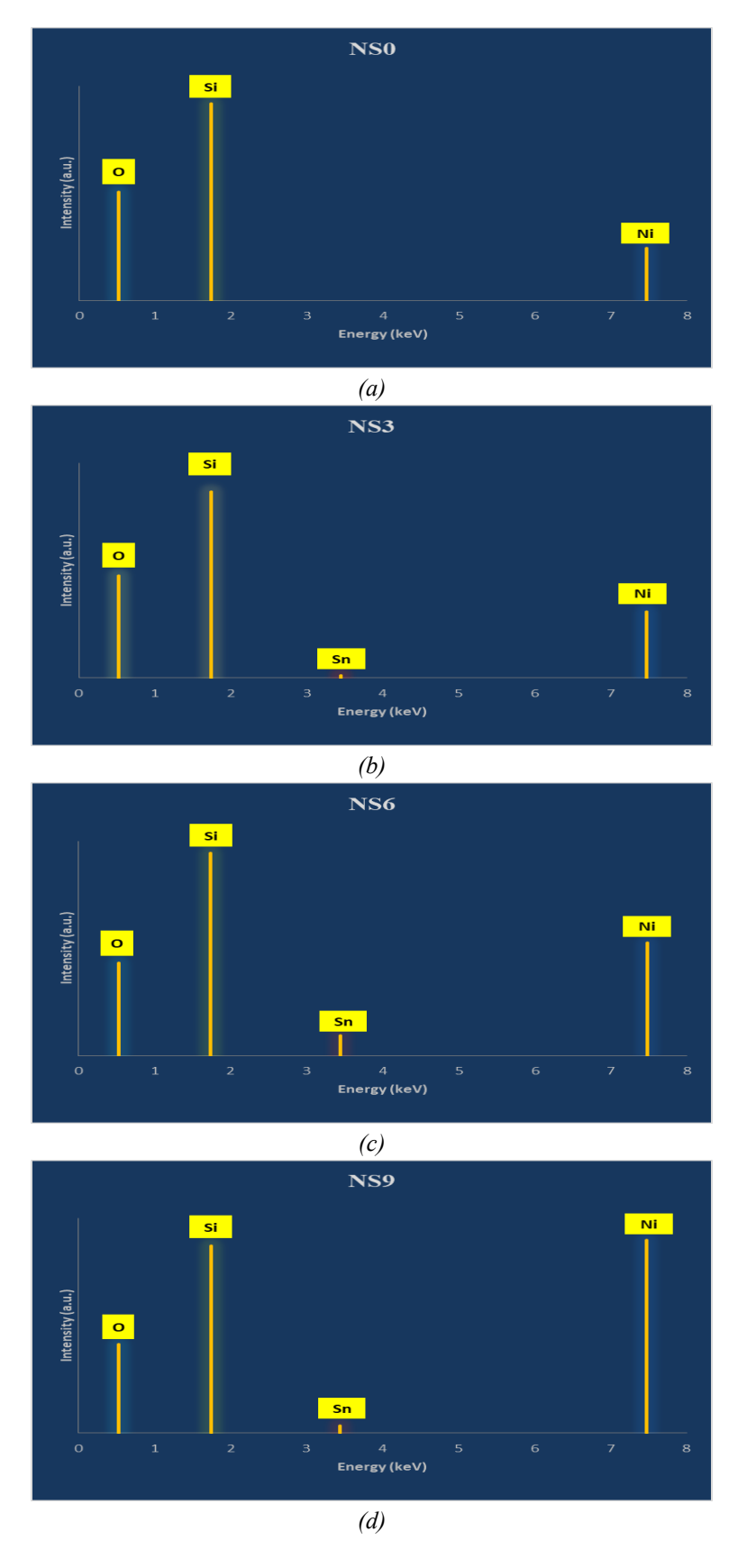


Fig. 8. The EDX spectrum of undoped and doped NiO thin films (a) NSO, (b) NS3, (c) NS6, (d) NS9.

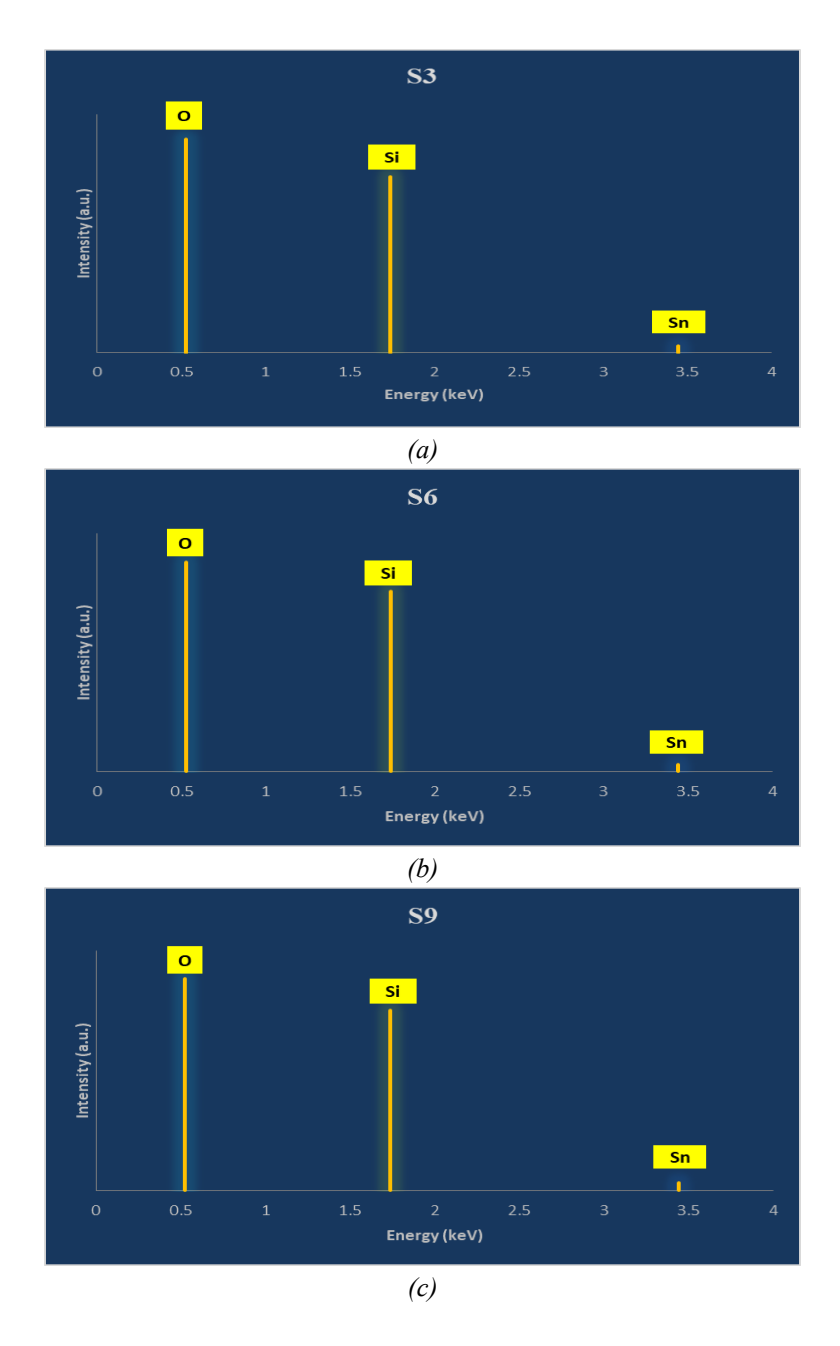


Fig. 9. The EDX spectrum of  $SnO_2$  films deposited by sublimation method (a) S3 (b) S6 (c) S9.

Table 2. The EDX spectrum of all deposited films.

| Samples  | NS0      | NS3      | NS6      | NS9      | S3       | S6       | S9       |
|----------|----------|----------|----------|----------|----------|----------|----------|
| elements | Weight % |
| Ni       | 14.7     | 18.6     | 26.4     | 40.4     | -        | -        | -        |
| Sn       | 0        | 0.7      | 4.7      | 1.6      | 1.8      | 1.8      | 2        |
| Si       | 55       | 52       | 47.3     | 39.2     | 44.4     | 45.4     | 45.1     |
| О        | 30.3     | 28.5     | 21.6     | 18.6     | 53.8     | 52.8     | 53       |

# 3.3. Optical properties

Figure 9 shows the transmission as a function of wavelength for undoped and Sn doped NiO prepared by spray pyrolysis. The figure shows that the transmission in general decreases with increasing Sn doping ratio. The slight increase in the transmission in sample NS9 compared with NS6 and NS6 may be due to sublimation of higher amount of Sn from this sample and this may create vacancies that allow a greater number of photons to transmit through the film.

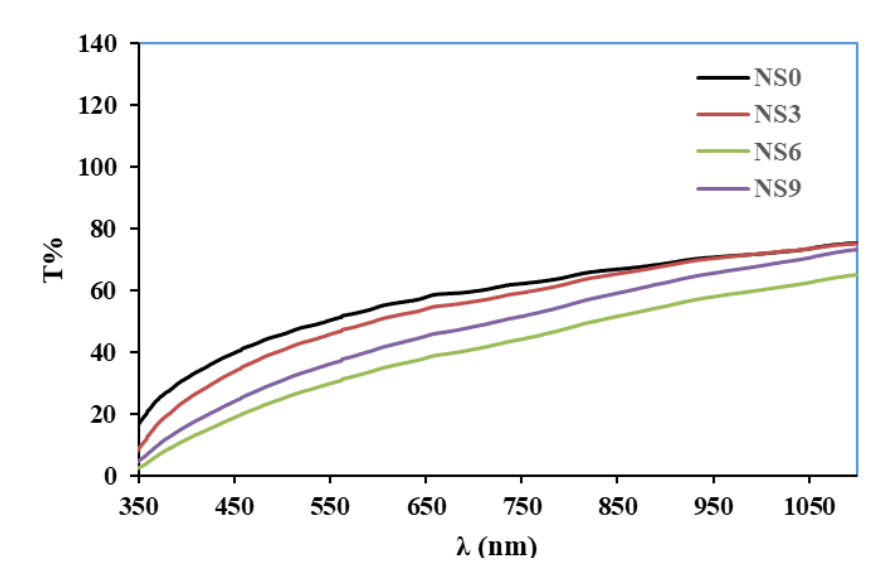


Fig. 9. Transmission spectrum of undoped and Sn doped NiO thin films prepared by CSP technique.

The absorption coefficient ( $\alpha$ ) is calculated as a function of the wavelength in the range (200-1200) for all prepared films using the following formula derived from Beer-Lambert law [44]:

$$\alpha = \frac{1}{d} \ln \frac{1}{T} \tag{3}$$

where *d* and *T* represent the film's thickness and transmission, respectively. Figure 10 shows the absorption coefficient's behavior relative to the doping ratio for selected wavelengths. The most significant effect occurs at 300 nm, as the corresponding photon energy at this point is larger than the thin film's energy gap, indicating band-to-band absorption. The absorption coefficient values align with Ref. [45].

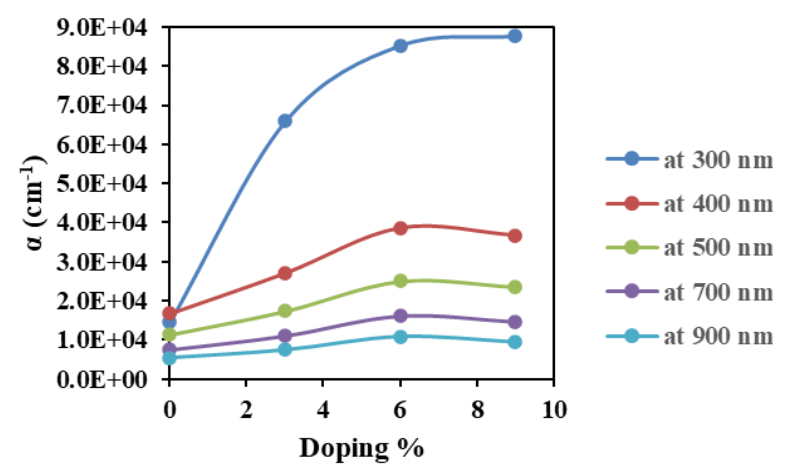


Fig. 10. Absorption coefficient as a function of doping ratio for NiO thin films prepared by CSP technique.

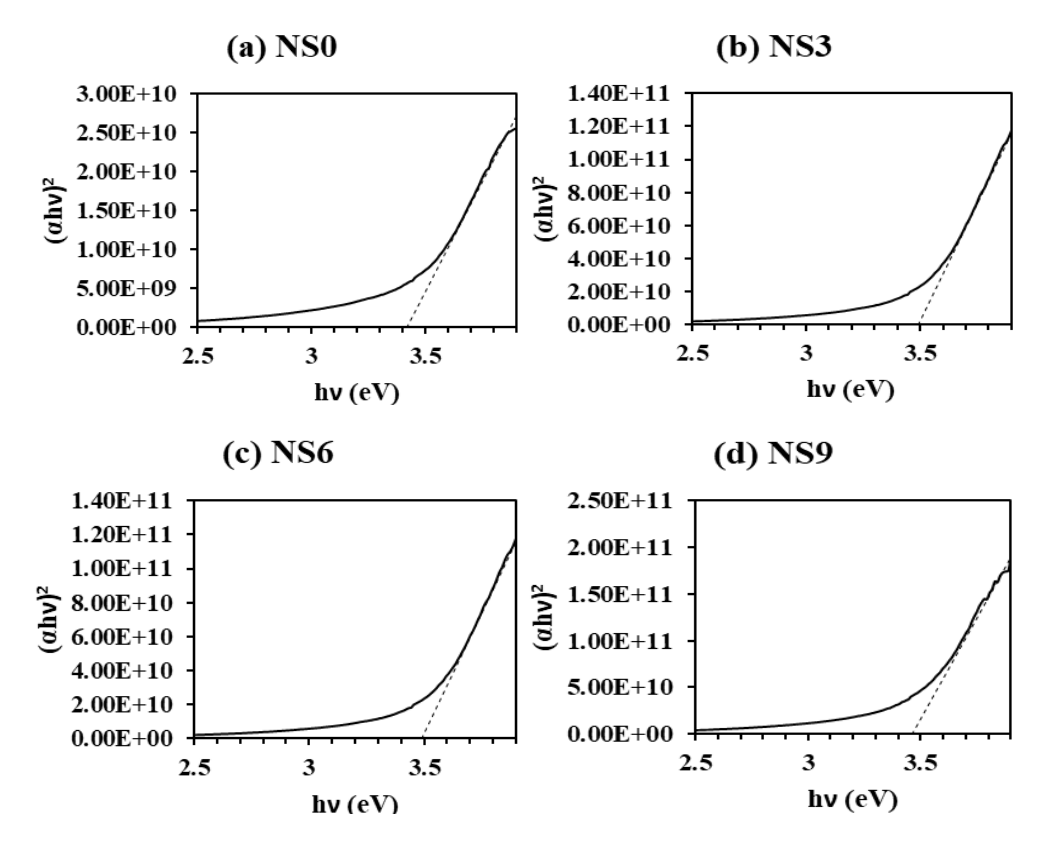


Fig. 11. Tauc plot  $(\alpha h v)^2$  Vs hv of all deposited thin films.

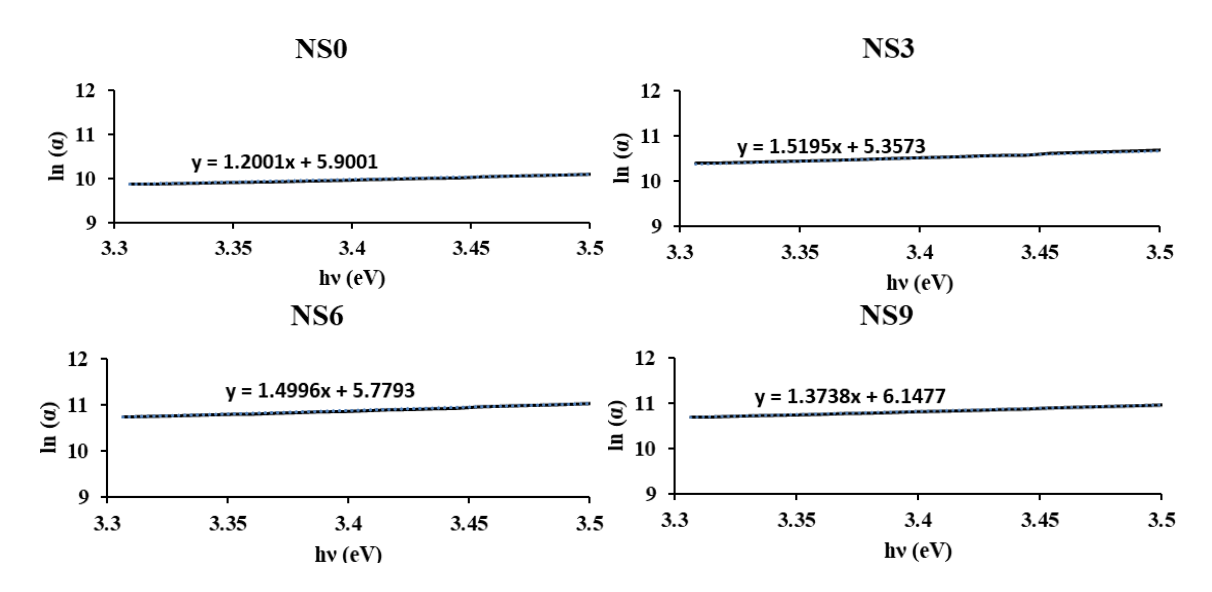


Fig. 12.  $Ln(\alpha)$  vs hv for doped and undoped NiO thin films.

Figure 11 illustrates the relationship between photon energy (hv) and  $(\alpha hv)^2$  for allowed direct electronic transitions. The values of the bandgap energy for Sn-doped NiO thin films are 3.42 eV, 3.49 eV, 3.46 eV, 3.44 eV for 0, 3, 6, and 9 % respectively. The crystallization was greatly reduced due to the defects generated by the sublimation of dopants. A decrease in the energy gap should be accompanied by an increase in the Urbach energy because of the formation of tails. However, it appears that the energy gap increases suddenly with 3% Sn-doping (NS3), and then it begins to decrease gradually with the doping 6% and 9%, (NS6 and NS9), also all energy gap values after doping are higher than the undoped sample (NS0). This may be to reduction in crystallinity

due to lattice distortions, or a new crystal phase has been created at the expense of vanishing of another phase. Moreover, it could be noted that no sharp absorption edges were observed, and this can be attributed to a high density of localized states in the energy bandgap of deposited thin films [46].

The Urbach energy was calculated for doped and undoped NiO films using Eq.(4) below [46,47].

$$\alpha = \alpha_0 \exp\left(\frac{h\nu}{E_0}\right) \tag{4}$$

where  $\alpha_0$  is proportionality constant, hv is the photon energy and  $E_u$  is the Urbach energy.

Figure 12 validates a linear relationship between (Ln $\alpha$ ) and photon energy ( $h\nu$ ). The Urbach energy is determined from the reciprocal of the slope in these graphs. This linearity confirms that Urbach energy is influenced by the localized states created within the bandgap due to the doping process.

| Sample        | Deposition method | Conditions  | E <sub>g</sub> (eV) | E <sub>u</sub> (eV) |
|---------------|-------------------|-------------|---------------------|---------------------|
| This work NS0 | CSP               | 0%Sn:NiO    | 3.42                | 0.833               |
| This work NS3 | CSP               | 3%Sn:NiO    | 3.49                | 0.658               |
| This work NS6 | CSP               | 6%Sn:NiO    | 3.46                | 0.667               |
| This work NS9 | CSP               | 9%Sn:NiO    | 3.44                | 0.728               |
| [47]          | CSP               | undoped NiO | 3.57                | 0.431-1.368         |
| [48]          | CSP               | undoped NiO | 3.51-3.54           | -                   |
| [49]          | RF snuttering     | RT 400C°    | 3 2-3 8             | 0.177 - 0.438       |

Table 3. Comparison between energy bandgaps and Urbach energy for Sn doped NiO thin films prepared by CSP technique.

Table 3 compares the energy bandgaps and Urbach energy for undoped and Sn-doped NiO films. The data in the table shows that, generally, the energy bandgap increases after doping, while the Urbach energies decrease. The unexpected lower value of  $E_g$  for 9% Sn:NiO may be due to the sublimation of higher amount of Sn atom. The values of  $E_g$  in this study are lower than those reported in References [47,48] for NiO thin films prepared by chemical spray pyrolysis. However, they are comparable to those found in Reference [49] for NiO prepared by sputtering.

### 4. Conclusion

As confirmed by x-ray diffraction test, highly crystalline NiO thin films can be successfully fabricated using low-cost spray pyrolysis, achieving structural quality comparable to films produced by RF sputtering. Sn doping significantly modifies the structural properties, leading to reduced optical transparency and an enhanced absorption coefficient-both advantageous for optoelectronic applications. FESEM analysis reveals a clear influence of **Sn** doping concentrations on surface morphology, with increasing irregularities observed at higher doping levels. Furthermore, the sublimation of Sn atoms from Sn -doped NiO films demonstrates potential as a novel, cost-effective approach for synthesizing SnO<sub>2</sub> thin films.

#### References

[1] M. Matsumiya, F. Qiu, W. Shin, N. Izu, N. Murayama, S. Kanzaki, Thin Solid Films 419(1-2), 213 (2002); https://doi.org/10.1016/S0040-6090(02)00762-9

- [2] H. T. Wang, D. K. Mishra, P. Chen, J. M. Ting, Journal of Alloys and Compounds 584, 142 (2014); https://doi.org/10.1016/j.jallcom.2013.08.142
- [3] F. H. Hsu, N. F. Wang, Y. Z. Tsai, Y. S. Cheng, M. P. Houng, Journal of Physics D: Applied Physics 46(27), 275104 (2013); <a href="https://doi.org/10.1088/0022-3727/46/27/275104">https://doi.org/10.1088/0022-3727/46/27/275104</a>
- [4] H. Wang, Z. Shi, B. Zhang, G. Wu, J. Wang, Y. Zhao, Journal of Luminescence 135, 160 (2013); https://doi.org/10.1016/j.jlumin.2012.10.024
- [5] M. A. Abbasi, Z. H. Ibupoto, M. Hussain, O. Nur, M. Willander, Nanoscale Research Letters 8, 1 (2013); <a href="https://doi.org/10.1186/1556-276X-8-320">https://doi.org/10.1186/1556-276X-8-320</a>
- [6] S. Chandramohan, K. Bok Ko, J. Han Yang, B. Deul Ryu, Y. S. Katharria, T. Yong Kim, C. H. Hong, Journal of Applied Physics 115(5), (2014); https://doi.org/10.1063/1.4863640
- [7] H. Long, L. Ai, S. Li, H. Huang, X. Mo, H. Wang, G. Fang, Materials Science and Engineering B 184, 44 (2014); <a href="https://doi.org/10.1016/j.mseb.2014.01.001">https://doi.org/10.1016/j.mseb.2014.01.001</a>
- [8] N. Park, K. Sun, Z. Sun, Y. Jing, D. Wang, Journal of Materials Chemistry C 1(44), 7333 (2013); <a href="https://doi.org/10.1039/c3tc31444h">https://doi.org/10.1039/c3tc31444h</a>
- [9] W. W. A. Bakar, M. Y. Othman, R. Ali, C. K. Yong, S. Toemen, Modern Applied Science 3(2), 36 (2009); <a href="https://doi.org/10.5539/mas.v3n2p35">https://doi.org/10.5539/mas.v3n2p35</a>
- [10] N. Shaigan, D. G. Ivey, W. Chen, Journal of the Electrochemical Society 156(6), B765 (2009); https://doi.org/10.1149/1.3116252
- [11] P. S. Patil, Materials Chemistry and physics, 59(3), 185-198(1999); https://doi.org/10.1016/S0254-0584(99)00049-8
- [12] S. Akinkuade, B. Mwankemwa, J. Nel, W. Meyer, Physica B: Condensed Matter, 535, 24-28(2018); https://doi.org/10.1016/j.physb.2017.06.021
- [13] X. Tang, Q. Yang, Journal of Electronic Materials 48, 7336-7344 (2019); https://doi.org/10.1007/s11664-019-07552-5
- [14] H. Sato, T. Minami, S. Takata, T. Yamada, Thin solid films 236(1-2), 27-31(1993); https://doi.org/10.1016/0040-6090(93)90636-4
- [15] P. Zhai, Q. Yi, J. Jian, H. Wang, P. Song, C. Dong, G. Zou, Chemical Communications 50(15), 1854-1856(2014); https://doi.org/10.1039/c3cc48877b
- [16] N. S. Sadeq, M. A. Hassan, Z. G. Mohammadsalih, Int. J. Thin Film Sci. Tec 11(1), 101-110 (2022); https://doi.org/10.18576/ijtfst/110113
- [17] L. Hu, R. H. Wei, X. W. Tang, W. J. Lu, X. B. Zhu, Y. P. Sun, Journal of Applied Physics 128(14) (2020); <a href="https://doi.org/10.1063/5.0023656">https://doi.org/10.1063/5.0023656</a>
- [18] A. Ainabayev, B. Walls, D. Mullarkey, D. Caffrey, K. Fleischer, C. M. Smith, I. Shvets, Scientific Reports 14(1), 1928 (2024); <a href="https://doi.org/10.1038/s41598-024-52024-4">https://doi.org/10.1038/s41598-024-52024-4</a>
- [19] A. N. Banerjee, K. K. Chattopadhyay, Progress in Crystal Growth and Characterization of Materials 50(1-3)52-105 (2005); https://doi.org/10.1016/j.pcrysgrow.2005.10.001
- [20] K. H. Kim, C. Takahashi, Y. Abe, M. Kawamura, Optik 125(12), 2899-2901 (2014); <a href="https://doi.org/10.1016/j.ijleo.2013.11.074">https://doi.org/10.1016/j.ijleo.2013.11.074</a>
- [21] J. D. Desai, Min S. K., K. D. Jung, O. S. Joo, Applied Surface Science, 253(4), 1781-1786(2006); <a href="https://doi.org/10.1016/j.apsusc.2006.03.009">https://doi.org/10.1016/j.apsusc.2006.03.009</a>
- [22] M. M. Ibrahim, M. A. Hassan, K. I. Hassoon, Bull Mater Sci 46, 120 (2023); https://doi.org/10.1007/s12034-023-02954-y
- [23] J. D. Desai. Journal of Materials Science: Materials in Electronics, 27(12), 12329-12334 (2016); <a href="https://doi.org/10.1007/s10854-016-5617-8">https://doi.org/10.1007/s10854-016-5617-8</a>
- [24] A. N. Hussain, K. I. Hassoon, M. A. Hassan. In Journal of Physics: Conference Series 1530(1) 012140(2020); https://doi.org/10.1088/1742-6596/1530/1/012140
- [25] R. S. Kate, S. C. Bulakhe, R. J. Deokate, Optical and Quantum Electronics, 51(10), 319 (2019); <a href="https://doi.org/10.1007/s11082-019-2026-2">https://doi.org/10.1007/s11082-019-2026-2</a>

- [26] L. Das, E. J. Canto-Aguilar, T. Tapani, H. Lin, H. Bhuvanendran, N. Boulanger, N. Maccaferri, Journal of Physics D: Applied Physics, 57(38), 385303 (2024); https://doi.org/10.1088/1361-6463/ad584a
- [27] P. S. Patil, L. D. Kadam, Applied Surface Science, 199(1-4), 211-221 (2002); <a href="https://doi.org/10.1016/S0169-4332(02)00839-5">https://doi.org/10.1016/S0169-4332(02)00839-5</a>
- [28] R. Sharma, A. D. Acharya, S. B. Shrivastava, T. Shripathi, V. Ganesan. Optik, 125(22), 6751-6756 (2014); https://doi.org/10.1016/j.ijleo.2014.07.104
- [29] S. M. Karadeniz, A. E. Ekinci, F. N. Tuzluca, M. Ertuprul, Asian J. Chem, 24(4), 1765-1768(2012).
- [30] M. Obaida, A. M. Fathi, I. Moussa, H. H. Afify, Journal of Materials Research 37(14), 2282-2292 (2022); <a href="https://doi.org/10.1557/s43578-022-00627-w">https://doi.org/10.1557/s43578-022-00627-w</a>
- [31] K. O. Ukoba, A. C. Eloka-Eboka, F. L. Inambao, Renewable and Sustainable Energy Reviews 82, 2900-2915 (2018); https://doi.org/10.1016/j.rser.2017.10.041
- [32] P. Salunkhe, M. A. AV, D. Kekuda, Applied Physics A 127(5), 390 (2021); https://doi.org/10.1007/s00339-021-04501-0
- [33] Y. Reddy, A. M. Reddy, A. S. Reddy, P. S. Reddy, J. Nano. Elect. Phy. 4(4) 04002(2012).
- [34] I. Hotový, D. Buc, Š. Haščík, O. Nennewitz, Vacuum 50(1-2), 41-44 (1998); https://doi.org/10.1016/S0042-207X(98)00011-6
- [35] A. M. Reddy, C. W. Byun, S. K. Joo, A. S. Reddy, P. S. Reddy, Electronic Materials Letters 10, 887-892 (2014); <a href="https://doi.org/10.1007/s13391-014-2181-3">https://doi.org/10.1007/s13391-014-2181-3</a>
- [36] A. Hakim, J. Hossain, K. A. Khan, Renewable Energy 34(12), 2625-2629 (2009); https://doi.org/10.1016/j.renene.2009.05.014
- [37] A. Bouhank, B. Youcef, S. Hacene, J. Chem. 12, 116-120 (2018).
- [38] B. G. Trabelsi, F. H. Alkallas, A. Ziouche, A. Boukhachem, M. Ghamnia, H. Elhouichet, Crystals 12(5), 692(2022); https://doi.org/10.3390/cryst12050692
- [39] A. L. Patterson, Physical Review 56(10), 978 (1939); https://doi.org/10.1103/PhysRev.56.978
- [40] P. Scherrer, Nach Ges Wiss Gottingen 2, 8-100 (1918).
- [41] G. K. Williamson, R. E. Smallman, Philosophical Magazine 1(1), 34-46 (1956); https://doi.org/10.1080/14786435608238074
- [42] J. I. Langford, A. J. C. Wilson, Journal of Applied Crystallography 11(2), 102-113 (1978); https://doi.org/10.1107/S0021889878012844
- [43] S. M. Menaka, G. Umadevi, Silicon 10(5), 2023-2029 (2018); https://doi.org/10.1007/s12633-017-9716-9
- [44] M. Fox, Optical Properties of Solids, Oxford University Press (2010).
- [45] Y. Liu, M. Liu, Advanced Engineering Materials 8(1-2), 89-93 (2006). https://doi.org/10.1002/adem.200500212
- [46] R. A. Ismail, A. M. Mousa, M. A. Hassan, Optik 179, 29-36 (2019); <a href="https://doi.org/10.1016/j.ijleo.2018.10.170">https://doi.org/10.1016/j.ijleo.2018.10.170</a>
- [47] M. M. Gomaa, M. Boshta, B. S. Farag, M. B. S. Osman, Journal of Materials Science: Materials in Electronics 27, 711-717 (2016); https://doi.org/10.1007/s10854-015-3807-4
- [48] M. S. Jamal, S. A. Shahahmadi, P. Chelvanathan, H. F. Alharbi, M. R. Karim, M. A. Dar, M. Akhtaruzzaman, Results in Physics 14, 102360 (2019); https://doi.org/10.1016/j.rinp.2019.102360
- [49] M. Aftab, M. Z. Butt, D. Ali, F. Bashir, T. M. Khan, Optical Materials 119, 111369 (2021); <a href="https://doi.org/10.1016/j.optmat.2021.111369">https://doi.org/10.1016/j.optmat.2021.111369</a>